EES Solar

PAPER

View Article Online
View Journal

Cite this: DOI: 10.1039/d5el00176e

Effect of RbF post-deposition treatment on open-circuit voltage in wide-gap (Ag,Cu)(In,Ga)Se_2 solar cells

Rico Gutzler, *[a] Saeed Bayat, [b] Dimitrios Hariskos,[a] Ana Kanevce, [a] Wolfram Hempel, [a] Stefan Paetel, [a] Susanne Siebentritt [b] and Wolfram Witte [a]

The compositional flexibility of the compound semiconductor (Ag,Cu)(In,Ga)Se_2 (ACIGS) allows fabricating thin-film solar cells with band gaps around 1.5 eV and above. These cells are well suited as top cells in tandem devices, for example together with silicon bottom cells, but also find use in photoelectrochemical energy conversion. However, current wide-gap ACIGS solar cells suffer from large open-circuit voltage losses, severely limiting their overall performance. Using an established inline ACIGS process with a standardized cell fabrication workflow, we explore different CdS buffer thicknesses, grown by chemical bath deposition on wide-gap ACIGS cells with a band gap ~1.5 eV. In addition, we systematically increase the RbF amount provided in post-deposition treatments. Quantum efficiency measurements, time-resolved and absolute steady-state photoluminescence help to understand the dependence of device performance on absorber composition and CdS buffer thickness. We observe a strong increase of the open-circuit voltage with RbF provided during post-deposition and concomitantly on charge carrier density as derived from capacitance–voltage measurements. Photoluminescence quantum yield likewise increases with increasing RbF amounts, leading to an increase in Quasi-Fermi level splitting. The highest charge carrier density is found in a cell with an open-circuit voltage exceeding 1000 mV at a an ACIGS band gap of 1.55 eV.

Received 24th October 2025
Accepted 22nd February 2026

DOI: 10.1039/d5el00176e

rsc.li/EESSolar

Broader context

Our study investigates the influence of the CdS buffer and RbF post-deposition treatments on wide band gap (~1.5 eV) (Ag,Cu)(In,Ga)Se_2 (ACIGS) thin-film solar cells. Increasing RbF treatment enhances open-circuit voltage, charge carrier density, and photoluminescence quantum yield, indicating improved quasi-Fermi level splitting. The optimized device achieves V_{OC} > 1.0 V at a band gap of 1.55 eV, demonstrating substantial mitigation of voltage losses in wide-gap ACIGS absorbers. This is the first report on a V_{OC} > 1 V with the commonly employed CdS buffer in ACIGS solar cells. The wide band gap investigated here is relevant for diverse applications, including as a top cell in tandem architectures, for indoor photovoltaics, and in photoelectrocatalysis.

Introduction

Chalcopyrite thin-film solar devices based on (Ag,Cu)(In,Ga)Se_2 (ACIGS) as absorber material have shown cell efficiencies exceeding 23% (ref. 1) and sub-module efficiencies above 20%.[2] Its band gap is adjustable between 1.0 and 1.8 eV (1.7 eV without Ag) depending on chemical composition and can be fine-tuned through the addition of silver.[3] ACIGS is hence a promising candidate material as a tandem partner. In particular the higher band gap range around 1.5 eV and above is interesting as a stable inorganic absorber in a thin-film top cell that can be combined with Si bottom cells. Widening the band gap to 1.5 eV is commonly achieved by increasing the [Ga]/([Ga] + [In]) (GGI) ratio by adding Ga up to GGI ≈ 80% in Se-based Cu(In,Ga)Se_2 (CIGS) absorbers, or by replacing Se partially or completely with sulfur. Both wide-gap Se-based CIGS and S-based Cu(In,Ga)S_2 are actively explored as photoabsorbers for photoelectrochemical energy conversion, an application in which high voltages are beneficial.[4–9] However, high open-circuit voltage (V_{OC}) losses currently contribute to the inferior performance of wide-gap ACIGS cells with GGI ratios close to 80% and a band gap around 1.5 eV compared to cells fabricated with a band gap of ~1.15 eV at GGI = 30%. The V_{OC} of record cells with GGIs ≈ 30% approach 90% of the maximum voltage dictated by the Shockley–Queisser (SQ) limit,[1] whereas best cells with a band gap of 1.44 eV currently only reach 80% of the SQ-limit and even less for wider band gaps.[10]

[a]Zentrum für Sonnenenergie- und Wasserstoff-Forschung Baden-Württemberg (ZSW), Meitnerstr. 1, 70563 Stuttgart, Germany. E-mail: rico.gutzler@zsw-bw.de
[b]Laboratory for Photovoltaics, Department of Physics and Materials Science Research Unit, University of Luxembourg, 41 rue du Brill, L-4422 Belvaux, Luxembourg

The treatment of wide-gap ACIGS absorbers and CIGS absorbers with heavy alkali metals is reported in several studies. An increase in V_{OC} as a consequence of reduced interface recombination is reported for CIGS cells with a GGI of around 80% that received a KF post-deposition treatment (PDT).[11] The same group then suggests the formation of a thin K(In,Ga)Se_2 surface layer with a lowered valence band maximum acting as a hole repellent that reduces interface recombination.[12] For pure $CuGaSe_2$ it was found that the V_{OC} remains unchanged upon RbF-PDT[13] but increases when supplying RbF during absorber growth.[7] For wide-gap ACIGS with GGI = 69–74% and high [Ag]/([Ag] + [Cu]) (AAC) ratios of 46–71%, an increase in V_{OC} is observed that goes hand in hand with a decrease in short-circuit current density (J_{SC}),[10] a typical observation for this material composition. This anticorrelation between voltage and current is described to originate from changes in doping concentration which in turn affects the space charge region width for absorbers with high Ag content.[14] Another way to increase the V_{OC} of $CuGaSe_2$ is the use of thicker CdS buffer layers, which is accompanied by an increased activation energy of the saturation current and hence reduced recombination.[7] Here, we explore these two different means that minimize V_{OC} losses in wide-gap ACIGS absorbers with a typical composition with GGI ≈ 80%, and a low AAC ≈ 6%, a composition so far not investigated with RbF-PDT. Cells prepared in our R&D line with mostly inline deposition steps[15] were subject to RbF-PDT showing that wide-gap ACIGS benefits from larger amounts of RbF compared to GGI = 30% cells. An alternative approach that boosts V_{OC} is the prolonged solution-growth of thicker CdS buffer layers compared to the standard 50 nm-thick CdS layer used at GGI = 30%. With either approach, V_{OC}s in the 950–990 mV range are routinely achieved, closing the gap to the highest reported V_{OC} of 1017 mV for pure $CuGaSe_2$ cells with a band gap close to 1.7 eV.[16] Distinct responses in external quantum efficiency (EQE), time-resolved photoluminescence (TRPL), and absolute steady-state photoluminescence (PL) measurements provide insight into V_{OC} loss mechanisms, charge carrier lifetimes, and quasi-Fermi level splitting and thus identify beneficial modifications for the development of high-V_{OC} devices. We observe a reduction of both radiative and non-radiative losses with increasing amount of RbF in the PDT process. Moreover, we find a strong dependence of V_{OC} on charge carrier density as derived from current–voltage measurements and observed the highest charge carrier density in a cell with V_{OC} = 1007 mV.

Methods

Solar cell fabrication

Wide-gap ACIGS solar cells and Ag-free standard CIGS with GGI = 32% for comparison were fabricated using a standardized work-flow as previously described.[17] Briefly, a ∼550 nm molybdenum layer was deposited by sputtering onto soda-lime glass substrates. The ACIGS absorber layer, approximately 2200 nm thick, was then co-evaporated using an inline coater with a multi-stage deposition process. Ag was co-evaporated with Cu in the second stage. The substrate heater temperature was set to a maximum of 720 °C in the third stage. Finally, rubidium fluoride was evaporated with the substrate heater set to 300 °C under selenium atmosphere in the inline machine without breaking the vacuum after the (A)CIGS deposition. The RbF amount was controlled by adjusting the source temperature, leaving the exposure time of the ACIGS absorber to the RbF flux constant. Several deposition runs were performed, in each one changing only the RbF source temperature in the specified range between 510–550 °C. The integral absorber composition within each run was held constant. Several of these deposition runs were performed, all showing quantitatively similar numbers and the same overall trends. Typical absorber compositions have a GGI = 75–82%, ([Ag] + [Cu])/([Ga] + [In]) ACGI = 70–80%, AAC = 4–7%, and band gaps E_g = 1.45–1.55 eV as extracted from EQE.

The CdS buffer layers were grown by chemical bath deposition (CBD) at 65, 80, and 90 °C using as precursors 1.4 mM $CdSO_4$, 1.5 M $NH_4(OH)$, and 0.1 M thiourea. The stated amounts are initial concentrations in the CBD reactor. Three different thicknesses were applied in solar cell devices, 50 nm, 100 nm, and 150 nm. The growth of the 50 nm layers was performed in one step with a deposition time of approximately 7 min. The thicker layers were realized after double or triple repetition of the 50 nm CBD process.

An ∼80 nm high-resistive layer of $Zn_{0.85}Mg_{0.15}O$ was then deposited on the buffer layer *via* RF sputtering, followed by a 280 nm Al-doped ZnO front contact, deposited by pulsed DC sputtering. Apart from the batch-based buffer deposition, all processing steps were carried out inline. Finally, a Ni/Al/Ni grid was applied using electron-beam evaporation, and mechanical scribing was used to define a total cell area of 0.5 cm^2. No anti-reflective coating was applied.

Materials and device characterization

The current density–voltage (*JV*) characteristics were measured using a WACOM Super Solar Simulator WXS-90S-L2 (grade AAA) under one sun AM1.5G illumination at 25 °C, calibrated with a silicon reference cell. EQE measurements were performed using a Bentham PVE300 system with a quartz-halogen lamp for white light biasing at a resolution of 5 nm, calibrated against a silicon reference cell. Elemental composition of the absorber layer was analyzed by X-ray fluorescence spectroscopy on a Fischerscope X-ray XDV-SDD, while vertical depth profiles were obtained using a time-of-flight secondary ion mass spectrometry (ToF-SIMS) with the M5 equipment by IONTOF GmbH. Time-resolved photoluminescence spectroscopy was conducted on a Picoquant FluoTime 300 with a 640 nm Laser and a repetition rate of 40 MHz, with measurements taken on the absorber/buffer structure within one hour after deposition. Control measurements on absorbers without CdS buffer did not show significant differences.

Absolute photoluminescence spectroscopy

Absolute PL spectroscopy was performed on ACIGS absorbers covered with the standard CdS buffer (∼50 nm thickness deposited at 65 °C) using a continuous-wave laser with an

excitation wavelength of 660 nm. The CdS buffer protects the surface from degradation due to oxidation in air.[18,19] The emitted photons were collected by two off-axis parabolic mirrors and guided to a spectrograph (Andor Shamrock SR-303i) through an optical fiber (550 μm in diameter). The detection was carried out using a silicon CCD camera (Andor iDus DV420A-OE) for the visible range and an InGaAs CCD camera (Andor iDus DU490A-1.7) for the infrared range.

To determine the absolute photon flux density, both spectral and intensity calibration were employed. During the spectral calibration step, a commercially available halogen lamp (Avantes AvaLight-HAL-CAL-Mini) was used. A spectralon, functioning as a near-ideal Lambertian reflector, was placed at the exact sample position and illuminated by the halogen lamp to mimic the PL emission of the samples. By comparing the detected reflected lamp spectrum with the standard lamp spectrum (provided by the manufacturer), a spectral calibration function was obtained. This calibration function corrected for all spectral distortions introduced by the collection system. Next, the intensity calibration was performed by directing the laser onto the spectralon and detecting the reflected laser with the spectrometer. By comparing the photon flux density extracted from the calibrated spectrum (measured by the spectrometer) with the real photon flux density of the laser (measured using a photodiode), an intensity calibration factor was derived. This factor makes the relative spectral correction absolute. All measurements were conducted under excitation photon flux densities corresponding to one sun, calculated based on the band gap of the material (*e.g.*, for a band gap of 1.5 eV, the one-sun photon flux density is 1.8×10^{17} cm^{-2} s^{-1}).

The quasi-Fermi level splitting (QFLS) values were extracted from the absolute PL spectra of the samples using generalized Planck law.[20] This involved a linear fit of the high-energy wing of the modified PL spectrum, with the temperature fixed at 296 K and taking into account the reflectance of the samples.[21,22]

To investigate radiative loss mechanisms in the films, the absorptance of the samples was extracted using generalized Planck law, using the QFLS obtained from the previous step. From the absorptance, the absorption coefficient ($\alpha(E)$) was calculated using the Beer–Lambert law, and the Urbach energy was extracted in the range where absorptance is well below 10^{-3}.[23] To evaluate total radiative losses in the samples, the band gap distribution function ($P(E_g)$) was determined as the first derivative of the absorptance.[24,25] The $P(E_g)$ function was then fitted to a Gaussian distribution to extract the band gap broadening parameter (σ_{E_g}), following the methodology detailed in ref. 21 and 26.

Results and discussion

The ACIGS absorbers show uniform grains in scanning electron microscopy (SEM) cross-sections with grain sizes larger than 1 μm and extending continuously from the Mo back contact to the front (Fig. 1 a). ToF-SIMS depth profiles show only a slight gradient with a GGI of approximately 80% up to 90% at the back contact Fig. 1b in five different measurements corresponding to different RbF-PDT temperatures.

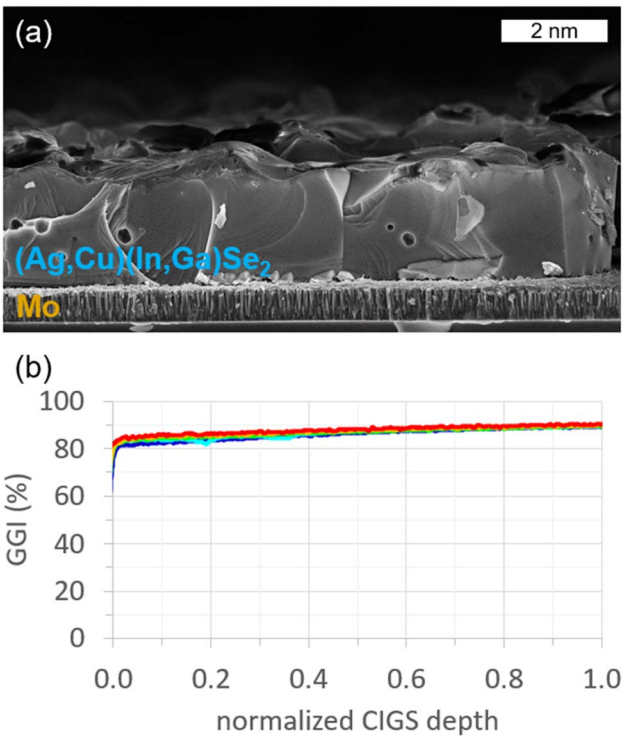

Fig. 1 (a) SEM cross-section of a typical wide-gap ACIGS absorber with a GGI of 78% with grain sizes >1 μm on a Mo/soda-lime glass substrate. (b) ToF-SIMS depth profiles of five absorbers with different RbF-PDT. All show a minor GGI gradient from front contact at a normalized depth of 0 up to the back contact at 1.0.

Motivated by the reported increase in V_{OC} for In-free $CuGaSe_2$ cells with increasing CdS thickness,[7] the chemical bath deposited CdS layer thickness was altered on wide-gap In-containing ACIGS absorbers. An increase from ~50 nm to ~100 and ~150 nm raises the V_{OC} on average by about 20 mV (see Fig. 2b), albeit at the cost of J_{SC} (Fig. 2c) due to parasitic absorption in the short-wavelength region (see EQE in Fig. 2f). Since also the fill factor (FF) increases with increasing buffer layer thickness (Fig. 2d), overall power conversion efficiency (PCE) is enhanced (Fig. 2a). Representative light *JV* curves are shown in Fig. 2e. As described previously, a possible explanation for this V_{OC} increase can be found in a direct correlation between activation energy and CdS buffer thickness and hence reduced recombination.[7] A conceivable cause for reduced interface recombination is diffusion of the constituents of the buffer into the absorber, changing interface properties through passivation and reducing interface recombination. Repeated CdS deposition steps as employed here and resulting longer buffer growth times would be in agreement with such an observation, *i.e.*, if in-diffusion occurs on the time scale of minutes. This hypothesis is corroborated by the observation that CdS layer deposited at increased temperatures (80 °C and 90 °C) also increase V_{OC} for a given thickness (Fig. 3). In comparison to ref. 7, however, which reports V_{OC} gains on the order of 150 mV by changing CdS thickness from 60 nm to 150 nm, the positive effect on V_{OC} found here is rather small.

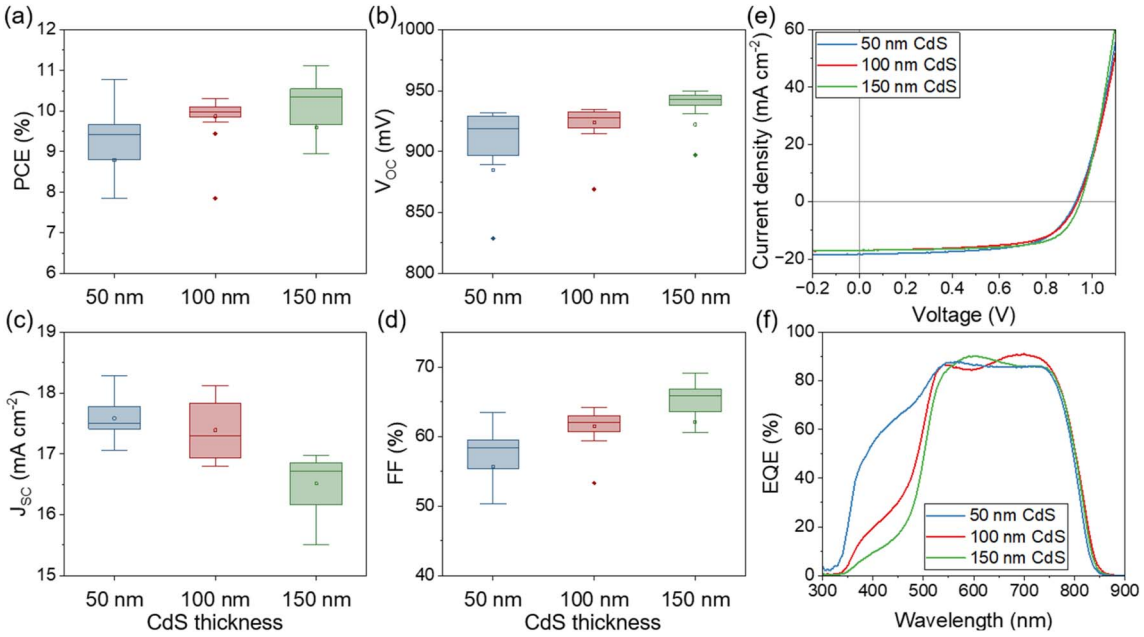

Fig. 2 (a) Power conversion efficiency, (b) open-circuit voltage, (c) short-circuit current density, and (d) fill factor of wide-gap ACIGS cells with GGI of 77% as a function of CdS layer thickness deposited at 65 °C. Each box includes 20 solar cells. (e) *JV* curves of representative solar cells with varying CdS layer thickness and (f) EQE of equally fabricated cells.

In contrast to the small gains in V_{OC} by increasing CdS layer thickness, larger optimization potential is observed in adjusting RbF-PDT. The dependence of V_{OC} and FF on RbF source temperature is shown in Fig. 4a for Ag-free CIGS cells with GGI = 32% in gray and wide-gap ACIGS cells with GGI = 76% in blue (band gap $E_g = 1.50$ eV estimated from EQE plots). V_{OC} increases with increasing RbF supply up to a point where both V_{OC} and FF suffer due to an excess of RbF. Wide-gap ACIGS requires higher RbF source temperatures of about 540 °C, *i.e.* a larger amount of RbF deposited onto the absorber, in order to maximize its V_{OC}, compared to GGI = 32% cells, which show a maximum in V_{OC} at 530 °C (see also ref. 27). For each 10 °C increment in RbF source temperature, the gain in V_{OC} is larger at GGI = 76%. TRPL confirms that the charge carrier lifetime in the wide-gap absorber increases with additional RbF-PDT (Fig. 4b, measured on ACIGS with CdS buffer layer). Lifetimes roughly double by increasing temperature from 510 °C to 550 °C. Nevertheless, the measured lifetimes with values below 2 ns are very low compared to values around 100 ns or above as observed on our standard CIGS samples with GGI around 30%.[17] Grain boundaries in the ACIGS absorber can be observed in the SEM image in Fig. 1a and are often suspected to be major recombination centers that can benefit from a larger amount of RbF. In addition, defects in the bulk absorber of wide-gap ACIGS that are not present or benign at lower Ga contents, for example deep Ga_{Cu} antisite defects,[28] might require better passivation by providing more RbF. The decrease in V_{OC} observed at a RbF-treatment at 550 °C is not explainable by the life-time increase and will be discussed further below.

A full picture of all *JV* data of the widegap ACIGS cells is presented in Fig. 5. Overall, PCE is independent of RbF source temperature up to a certain point (540 °C), after which it sharply drops mainly due to reduced FF and V_{OC} values. Also apparent in Fig. 5b and c is the dependence of V_{OC} on RbF temperature

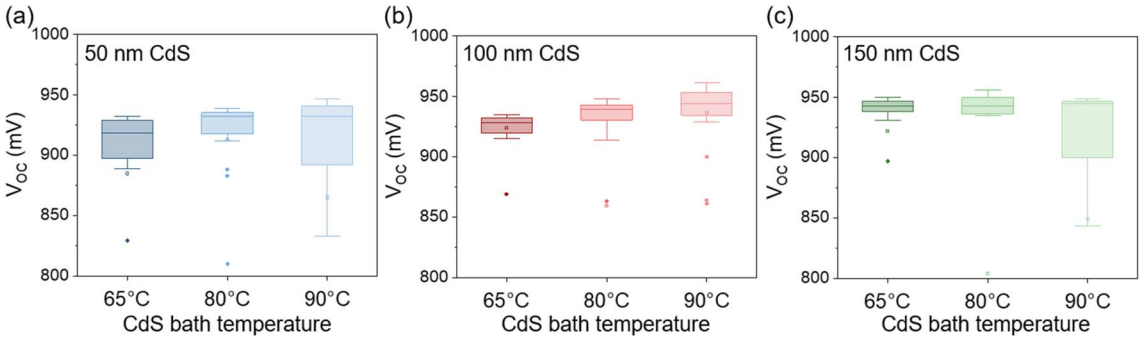

Fig. 3 Open-circuit voltage dependence on CdS bath temperature for (a) 50 nm thick CdS, (b) 100 nm thick CdS, and (c) 150 nm thick CdS. Each box includes 20 solar cells.

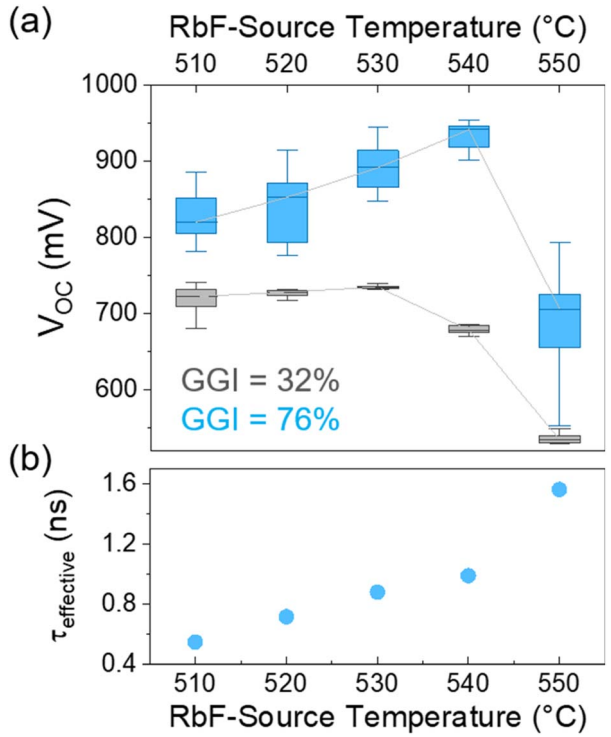

Fig. 4 (a) V_{OC} dependence on RbF source temperature of Ag-free standard CIGS cells with GGI = 32% (gray) and wide-gap ACIGS cells with GGI = 76% (blue). (b) Effective charge carrier lifetime from time-resolved photoluminescence measurements as a function of RbF source temperature of ACIGS cells with GGI = 76%.

and the low V_{OC} for high RbF supply, as likewise observed for GGI ~30% cells previously.[27] Absorber material with RbF deposited at 550 °C shows low V_{OC} and low FF (Fig. 5b and c), which is reflected in the non-ideal *JV* curve in Fig. 6a (red). An anti-correlation between J_{SC} and V_{OC} is observed, where more RbF leads to an increasing V_{OC} and decreasing J_{SC}. Keller and coworkers observed such an anti-correlation as a function of absorber stoichiometry and argue that changes in doping concentration alter space charge region (SCR) width and hence carrier collection.[14] They argue that very low diffusion lengths (compare also carrier life times in Fig. 4b) require wide SCR, which increases when going towards stoichiometry. Representative *JV* curves of cell from Fig. 5 are shown in Fig. 6.

The chemical composition and hence stoichiometry of the here presented absorbers, however, is constant such that the integral GGI, ACGI, and AAC values as measured by X-ray fluorescence measurements do not change. CV data (not shown) exhibit that doping density N_a increases with increasing RbF amount up to 540 °C and space charge width (SCW) decreases. Above this temperature, N_a abruptly decreases and SCW increases. Clearly, more Rb in the absorber results in higher doping, leading to higher V_{OC}, with the expected reduction in SCW and poorer carrier collection due to the very low carrier lifetime, resulting in low J_{SC}. A V_{OC} *vs.* N_a plot in Fig. 6b highlights the dependence of voltage on carrier density for five RbF source temperatures, the N_a extracted from *CV* measurements correspond to best-performing cells and the V_{OC} to cells with highest voltage as shown in Fig. 6a (same color code). The sixth

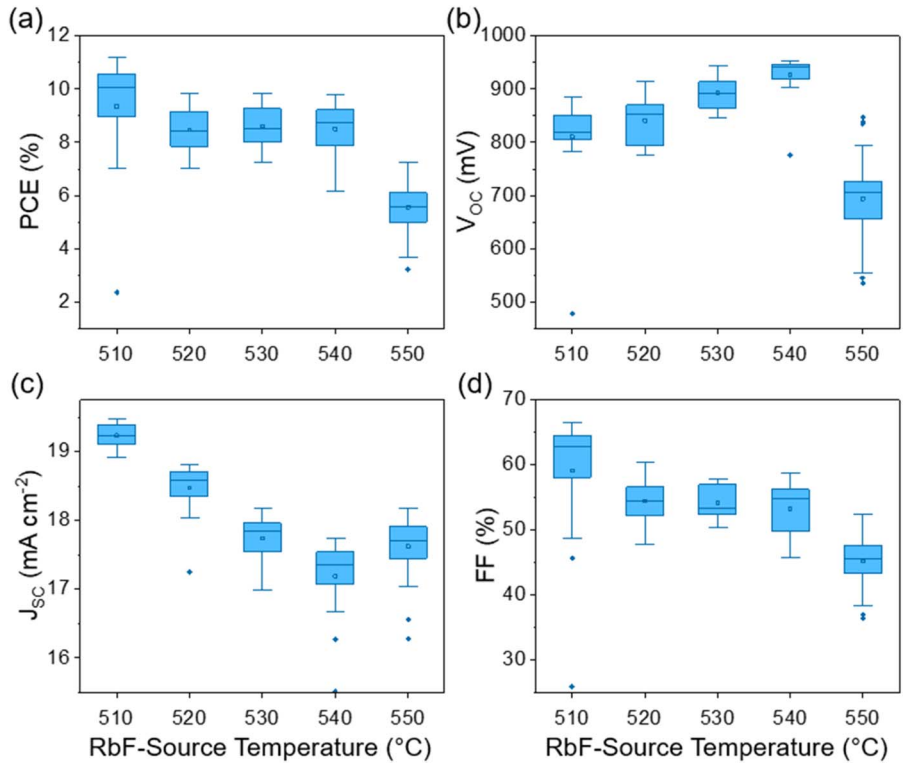

Fig. 5 Box plots of *JV* data of wide-gap ACIGS cells with GGI around 76%, 50 nm thick CdS buffer deposited at 65 °C, as a function of RbF source temperature. (a) PCE, (b) V_{OC}, (c) J_{SC}, and (d) FF.

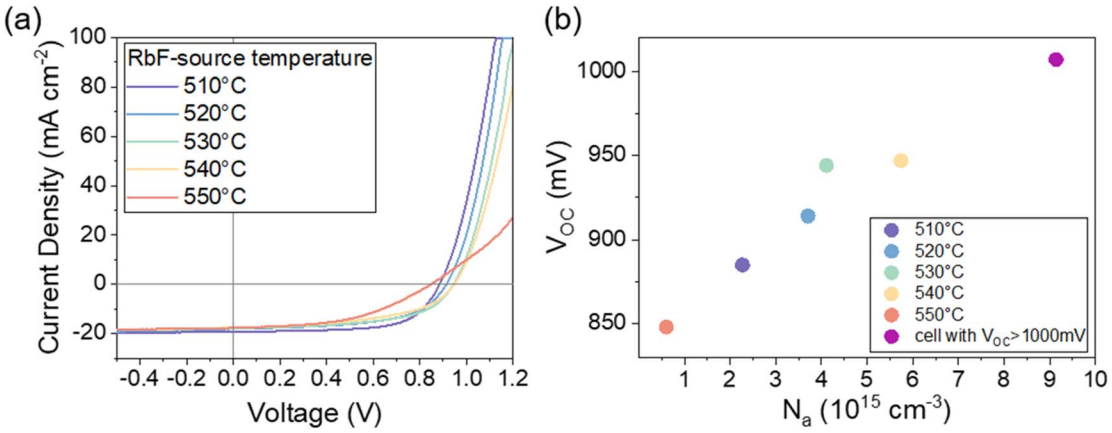

Fig. 6 (a) Representative light *JV* curves of wide-gap ACIGS cells with GGI around 76%, 50 nm thick CdS buffer (65 °C), as a function of RbF source temperature. (b) V_{OC} as a function of carrier density, same color code as in (a). The magenta dot marks the cell with V_{OC} > 1000 mV.

data point in magenta to the right corresponds to a cell prepared in a different deposition run and depicts the highest V_{OC} we achieved of 1007 mV with an ACIGS absorber with a band gap of 1.55 eV. This is substantially higher than commonly reported V_{OC} values at this band gap with values <950 mV (ref. 10) and closes in to the highest reported V_{OC}s > 960 mV and up to 1017 mV for pure $CuGaSe_2$.[7,16,29] Also here, the high V_{OC} is accompanied by a low J_{SC} of 16.2 mA cm^{-2}. A doping density approaching 10^{16} cm^{-3} is required to achieve such a high V_{OC}.

The trend observed in V_{OC} in Fig. 4 and 5 appears to be in line with expectations from the observed trend in doping, but the cell with the RbF temperature of 550 °C contradicts the trend in minority carrier lifetime (Fig. 4b). To better understand the origin of the V_{OC} variation with RbF source temperature, we consider the combined effect of lifetime τ and doping level N_A on the open-circuit voltage *via* the quasi-Fermi level splitting ΔE_F, *i.e.* the internal voltage.[22] The bulk recombination rate R^b is inversely proportional to the product of lifetime and doping density $R^b \propto (\tau \cdot N_A)$ and interface recombination rate R^i scales linearly with the surface recombination velocity $R^i \propto S_h$.[30] We use the sample processed at 510 °C as a reference, and calculate the expected ΔE_F change due to bulk recombination R^b based on lifetime (Fig. 4b) and doping level (Fig. 6b):

$$\delta\Delta E_F \approx kT \ln\left(\frac{\tau \cdot N_A}{\tau_{510} \cdot N_{A,510}}\right)_j$$

Table 1 presents the values of the expected $\delta\Delta E_F$ and the observed ΔV_{OC} as a function of RbF source temperature. The trend in expected ΔE_F and in observed V_{OC} is the same: increase up to 540 °C RbF temperature and then a decrease. This indicates that part of the V_{OC} changes can indeed be explained by the trends in doping level and minority lifetime and that the decreased doping level for 550 °C outweighs the increase in lifetime. However, the observed increase in V_{OC} is much larger than predicted by changes in bulk recombination R^b alone: the increase with increasing RbF temperature up to 540 °C is stronger and the decrease with higher RbF temperature is also more drastic than expected from lifetime and doping level. This discrepancy can be attributed to changes in interface recombination R^i.[22,31] This recombination path can cause a gradient in the minority carrier Fermi level and thus affect V_{OC} much stronger than ΔE_F. This interpretation implies that RbF treatments with a source temperature up to 540 °C improve the interface, *i.e.*, reduce interface recombination, whereas RbF with source temperature of 550 °C is detrimental for the interface and causes increased interface recombination.

Tunneling recombination has been discussed as a limiting recombination pathway in particular for wide-gap CIGS.[32] This recombination pathway can be excluded from having a dominant contribution. The tunneling rate $R^t \propto n_d \exp(-1/E)$ depends linearly on (defect) states at the interface n_d and exponentially on $-1/E$, where $E = V/\mathrm{SCW}$ is the electric field in the pn-junction with potential V and SCW. The addition of Rb is expected to lower n_d while the smaller SCW (which scales inversely with Na, see also Fig. 6b) with increasing amounts of Rb will increase the electric field. Tunnelling recombination will increase with more Rb, which is opposite to the observed decrease in overall recombination, and hence does not significantly contribute.

In order to study the role of RbF post-deposition treated absorbers the quasi-Fermi level splitting, absolute PL spectroscopy was performed on the second batch of absorbers covered by a protective CdS buffer layer. Fig. 7a shows the PL spectra of different RbF-treated absorbers on a semi-logarithmic scale. Notably, the PL quantum yield increases consistently with higher RbF supply, and this trend persists even for the sample treated with an RbF source temperature of

Table 1 V_{OC} and QFLS improvement of RbF post-treated samples as a function of increasing RbF source temperature

RbF source temperature (°C)	510	520	530	540	550
Lifetime τ (ns) (Fig. 4b)	0.55	0.72	0.88	0.99	1.56
N_A (cm^{-3}) (Fig. 6b)	2.3	3.7	4.1	5.7	0.6
$\Delta V_{OC,max}$ (mV)	0	29	59	62	−37
$\delta\Delta E_F$ (meV)	0	19	26	36	−8

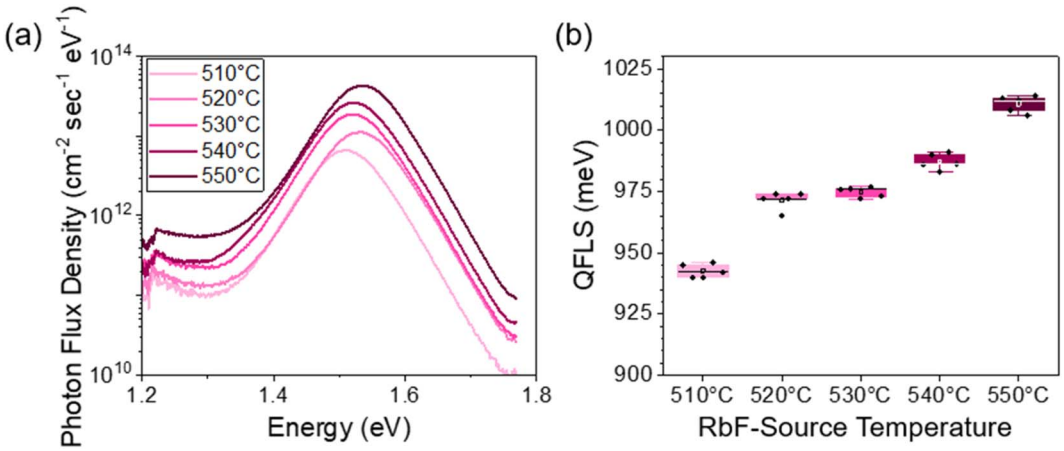

Fig. 7 Dependence of (a) PL spectra and (b) QFLS of wide-gap ACIGS absorbers on RbF source temperature.

550 °C. The extracted quasi-Fermi level splitting ΔE_F of these samples follows a similar trend, exceeding 1000 meV at the highest RbF dose. Solar cells made from this second run show a similar trend in V_{OC}: increase up to 975 mV at an RbF source temperature of 550 °C, indicating that the decrease in doping and the degradation of the interface at this source temperature are not universal und subject to minor process variations.

Moreover, it can be seen in Table 2 that the increase in V_{OC} as a function of RbF dose is stronger than the increase in ΔE_F. The difference between ΔE_F and V_{OC} can be attributed to interface recombination.[31] This loss ($\Delta E_F - qV_{OC}$) is about 110 meV at RbF temperatures of 510 °C and 520 °C and reduces to 70–80 meV at 530 °C and 540 °C and finally reaches 35 meV for 550 °C. This reduction of the interface loss hints that the RbF treatment improves the absorber–buffer interface with increasing RbF temperature. The improvement in both non-radiative recombination and minority carrier lifetime, along with the improvement in interface losses, indicates that RbF-PDT has a positive impact on both bulk and interface properties of the absorber. However, it can be seen that the RbF-treated sample at 550 °C in this run showed completely different behavior than its counterpart in its first run, and no voltage drop was observed in this case. The reason for this different behavior is not understood yet, but it can be explained by sample-to-sample variability within different batches.

To investigate radiative losses in RbF-treated ACIGS absorber layers, Urbach energy (E_U) and band gap broadening (σ_{E_g}) parameters were extracted from the PL spectra as detailed in the experimental section and are shown in Fig. 8. The data reveal that with increasing doses of heavy alkali elements during the PDT process, the E_U value of the absorber layer slightly decreases. The decrease is not monotonous but a general trend can be observed, in agreement with observations in the literature.[33] This decline in Urbach energy describes a reduction in the density of sub-band gap tail states, which can be partly due to the higher doping level, which reduces electrostatic fluctuations,[34] and partly due to an improvement of structural disorder.[35] A reduction in tail states leads to an improvement of radiative and non-radiative V_{OC} losses and thus contributes to higher QFLS and V_{OC}.[23]

A similar but more pronounced trend is observed for σ_{E_g}, where higher RbF content during the PDT process reduces the absorption edge broadening of the absorber layer. It is interesting to note that for this sample series there is a clear correlation between Urbach energy and absorption edge broadening. This correlation was observed before in samples fabricated in the same laboratory[15] but is not necessarily the case when comparing cells from different laboratories.[36–38] The correlation observed here is a hint that, in this case, the absorption edge broadening is partly due to disorder and Urbach tails.

The general conclusion from the PL investigation is that increased RbF treatment improves the absorber bulk and reduces non-radiative recombination channels, increasing lifetime and QFLS.

Table 2 V_{OC} and QFLS values of RbF post-treated samples as a function of increasing RbF source temperature

RbF source temperature (°C)	510	520	530	540	550
V_{OC} (mV)	833	868	900	908	975
$QFLS_{PL}$ (meV)	944	974	977	990	1010

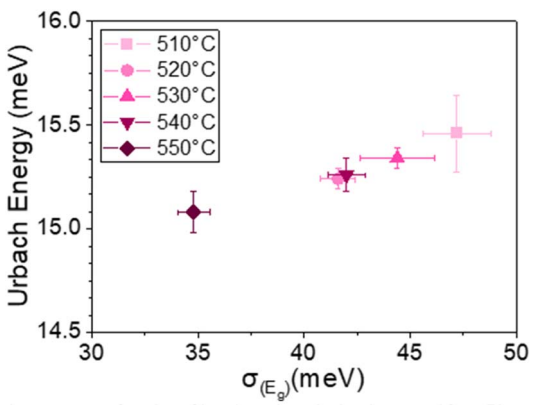

Fig. 8 Urbach energy as a function of band gap broadening (extracted from PL spectra) for wide-gap ACIGS absorbers with different RbF source temperature.

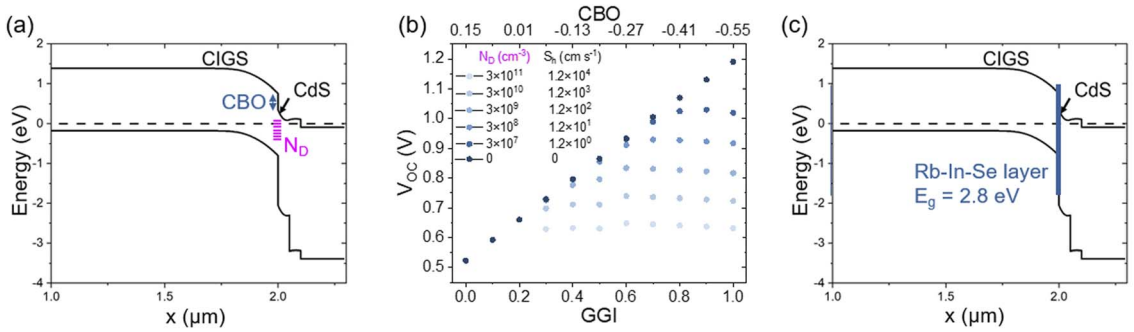

Fig. 9 (a) A simulated equilibrium band diagram of a wide-gap ACIGS cell with 1.5 eV band gap. A cliff-like configuration is appreciable at the absorber/buffer interface with a pronounced CBO. (b) Simulated V_{OC} for different interface defect densities as a function of the GGI in absorber. For V_{OC}s approaching 1 V for high GGIs, very low recombination rates are required. (c) Band diagram of the same junction depicted in (a) with a speculative wide-gap Rb–In–Se surface layer that passivates the interface.

Apart from a beneficial effect of RbF-PDT by increasing doping density and by reducing recombination in the bulk (point defects and grain boundaries), the RbF treated absorber/buffer interface of ACIGS cells warrants a closer inspection. Recent X-ray and ultraviolet photoelectron spectroscopy experiments on the Ag-free CIGS/CdS interface of a GGI 90% absorber with RbF-PDT measured a cliff of −0.53 eV that contributes significantly to the V_{OC}-deficit *vs.* the band gap ($E_g/e - V_{OC}$) of 770 mV.[39] The samples described here have a GGI of around 80% such that the conduction band minimum is lower and concomitantly the cliff smaller, see Fig. 9a for a tentative band diagram. In addition, Ag-alloying further lowers the conduction band minimum,[3] although with low AACs of ~7% used here this amounts to only a few tens of meV. Taken together, lowering slightly the GGI and adding Ag to the absorber reduces the cliff at a CIGS/CdS interface, reducing some of the V_{OC} losses. The V_{OC}-deficit with respect to the SQ-limit amounts to 270 mV in the cell with E_g = 1.55 eV and V_{OC} = 1007 mV (V_{OC}-deficit of 543 mV *vs.* the band gap). Another cell has an even smaller deficit of 260 mV at E_g = 1.52 eV (V_{OC}-deficit of 529 mV *vs.* the band gap). Both cells are close to 80% of the SQ-limit. These comparably low losses are likely not only due to reduced bulk recombination and a lower conduction band cliff but most likely additional factors are at play. Fig. 9b shows a SCAPS-1D[40] simulation of the V_{OC} as a function of GGI for different interface defect densities N_D and interface recombination rates. Clearly, for a V_{OC} of 1 V, the interface recombination rate must be very low, *i.e.*, interface passivation must be very efficient. This can be achieved by a thin layer of a wide-gap material at the absorber/buffer interface. A Rb–In–Se layer at the absorber/buffer interface is proposed for RbF-treated wide-gap ACIGS cells,[10] which due to its wide band gap around 2.8 eV (ref. 41) could reduce recombination at the interface and increase V_{OC} if the layer's band gap and band alignment is favorable. Such a Rb–In–Se layer was shown to form at our ACIGS samples with similar AAC around 7% with lower GGI around 30%[42] but currently remains speculative for the wide-gap ACIGS cells presented here. However, the presence of such a layer and whose thickness might depend on the provided amount of RbF is a viable candidate that explains reduced interface recombination, see Fig. 9c for a band diagram. The blocking-like *JV* curves once too much RbF is present might then be a consequence of a Rb–In–Se layer that became too thick.

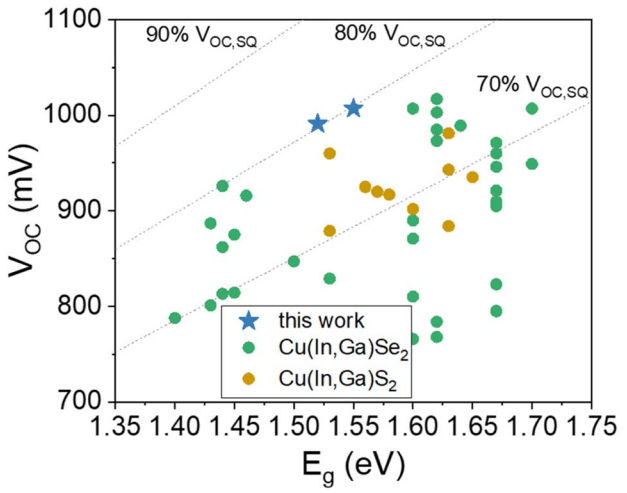

Fig. 10 V_{OC} *vs.* E_g plot of reported values. Blue stars: selected ACIGS cells of this work with ~80% of the SQ-limit, green: Se-based (A)CIGS cells,[3,7,10,14,16,29,44–53] orange: S-based Cu(In,Ga)S_2 cells.[54–60] The dotted lines show the 70%, 80%, and 90% values of the SQ-limit.

The ACIGS cells with highest V_{OC} with E_g > 1.5 eV are close to 80% of the achievable V_{OC} dictated by the SQ-limit (SQ data taken from ref. 43) and compare favorably with other wide-gap cells reported in the literature (see Fig. 10), whether it be selenides or sulfides, for band gaps between 1.4 and 1.7 eV.

Conclusions

Our data highlights ways towards improved ACIGS cells with a band gap around 1.5 eV for applications where a high V_{OC} is desirable. We show that optimized RbF-PDT procedures and increased solution-grown CdS buffer thickness and bath temperature can be useful in improving device performance. Up to band gaps of 1.55 eV, or possibly even higher, CdS can be a suitable n-partner for wide-gap ACIGS solar cells, allowing for cells with V_{OC} of 1007 mV. High amounts of RbF increase

doping at the cost of space charge region width, leading to an anticorrelation of V_{OC} and J_{SC}. The comparison between V_{OC} and QFLS suggests that RbF treatment reduces interface recombination. The formation of a Rb–In–Se layer between absorber and buffer is suggested as a possible reason and is a worthwhile candidate for future (spectroscopic) investigations. Although increasing the RbF source temperature up to 550 °C improved both radiative and non-radiative losses in the ACIGS/CdS-based cells, a significant decline in V_{OC} was observed at 550 °C source temperature. This finding suggests that an excessive dose of RbF may introduce new recombination channels, particularly at the interface, which are detrimental for device performance.

Author contributions

R. G.: conceptualization, methodology, investigation, data curation, writing – original draft preparation, writing – review and editing. S. B. investigation, data curation, methodology, writing – review and editing. D. H. investigation, data curation, writing – review and editing. A. K. investigation, data curation, writing – review and editing. W. H. investigation, data curation, writing – review and editing. S. P. writing – review and editing S. S. methodology, supervision, project administration, funding acquisition, writing – review and editing. W. W. conceptualization, project administration, funding acquisition, writing – review and editing.

Conflicts of interest

There are no conflicts to declare.

Data availability

Data for this article are available at Zenodo at https://doi.org/10.5281/zenodo.18798240.

Acknowledgements

This project has received funding from the European Union program HORIZON (Call: HORIZON-CL5-2021-D3-02), Project ID: 101075626 (SITA). Funded by the European Union. Views and opinions expressed are however those of the author(s) only and do not necessarily reflect those of the European Union or CINEA. Neither the European Union nor the granting authority can be held responsible for them.

References

1 J. Keller, K. Kiselman, O. Donzel-Gargand, N. M. Martin, M. Babucci, O. Lundberg, E. Wallin, L. Stolt and M. Edoff, High-concentration silver alloying and steep back-contact gallium grading enabling copper indium gallium selenide solar cell with 23.6% efficiency, *Nat. Energy*, 2024, (9), 467–478, DOI: 10.1038/s41560-024-01472-3.

2 H. ElAnzeery, M. Stölzel, P. Eraerds, P. Borowski, H. Aboulfadl, A. Lomuscio, D. Helmecke, C. Schubbert, S. Oueslati, M. Hála, J. Röder, F. Giesl and T. Dalibor, Beyond 20% World Record Efficiency for Thin-Film Solar Modules, *IEEE J. Photovoltaics*, 2024, **14**(1), 107–115, DOI: 10.1109/JPHOTOV.2023.3326559.

3 J. Keller, K. V. Sopiha, O. Stolt, L. Stolt, C. Persson, J. J. Scragg, T. Törndahl and M. Edoff, Wide-gap (Ag,Cu)(In,Ga)Se_2 solar cells with different buffer materials - A path to a better heterojunction, *Prog. Photovolt.: Res. Appl.*, 2020, **28**(4), 237–250, DOI: 10.1002/pip.3232.

4 S. Ikeda, R. Okamoto and S. Ishizuka, Enhancement of the photoelectrochemical properties of a $CuGaSe_2$-based photocathode for water reduction induced by loading of a Cu-deficient layer at the p–n heterointerface, *Appl. Phys. Lett.*, 2021, **119**, 083902, DOI: 10.1063/5.0060494.

5 N. Gaillard, D. Prasher, M. Chong, A. Deangelis, K. Horsley, H. A. Ishii, J. P. Bradley, J. Varley and T. Ogitsu, Wide-Bandgap Cu(In,Ga)S_2 Photocathodes Integrated on Transparent Conductive F:SnO_2 Substrates for Chalcopyrite-Based Water Splitting Tandem Devices, *ACS Appl. Energy Mater.*, 2019, **2**(8), 5515–5524, DOI: 10.1021/acsaem.9b00690.

6 J. C. Carter, D. Hauschild, L. Weinhardt, K. Horsley, D. Hariskos, N. Gaillard and C. Heske, Electronic Structure of Chalcopyrite Surfaces for Photoelectrochemical Hydrogen Production, *J. Phys. Chem. C*, 2023, **127**(17), 8235–8246, DOI: 10.1021/acs.jpcc.2c09063.

7 S. Ishizuka, R. Okamoto and S. Ikeda, Enhanced Performance of Ternary $CuGaSe_2$ Thin-Film Photovoltaic Solar Cells and Photoelectrochemical Water Splitting Hydrogen Evolution with Modified p–n Heterointerfaces, *Adv. Mater. Interfaces*, 2022, **9**(25), 2201266, DOI: 10.1002/admi.202201266.

8 Y. Liu, M. Xia, D. Ren, S. Nussbaum, J.-H. Yum, M. Grätzel, N. Guijarro and K. Sivula, Photoelectrochemical CO_2 Reduction at a Direct $CuInGaS_2$/Electrolyte Junction, *ACS Energy Lett.*, 2023, **8**(4), 1645–1651, DOI: 10.1021/acsenergylett.3c00022.

9 J. Guerrero, E. Bajard, N. Schneider, F. Dumoulin, D. Lincot, U. Isci, M. Robert and N. Naghavi, Multifunctional Photovoltaic Window Layers for Solar-Driven Catalytic Conversion of CO_2: The Case of CIGS Solar Cells, *ACS Energy Lett.*, 2023, **8**(8), 3488–3493, DOI: 10.1021/acsenergylett.3c01205.

10 J. Keller, H. Aboulfadl, L. Stolt, O. Donzel-Gargand and M. Edoff, Rubidium Fluoride Absorber Treatment for Wide-Gap (Ag,Cu)(In,Ga)Se_2 Solar Cells, *Sol. RRL*, 2022, **6**(6), 2200044, DOI: 10.1002/solr.202200044.

11 S. Zahedi-Azad and R. Scheer, Quenching interface recombination in wide bandgap Cu(In,Ga)Se_2 by potassium treatment, *Phys. Status Solidi C*, 2017, **14**(6), 1600203, DOI: 10.1002/pssc.201600203.

12 S. Zahedi-Azad, *Characterization of Alkaline-Doped Wide Bandgap Chalcopyrite Cu(In,Ga)Se2 Thin Films and Solar Cells*, DOI: 10.25673/35172.

13 S. Ishizuka, N. Taguchi, J. Nishinaga, Y. Kamikawa, S. Tanaka and H. Shibata, Group III Elemental Composition Dependence of RbF Postdeposition

Treatment Effects on Cu(In,Ga)Se_2 Thin Films and Solar Cells, *J. Phys. Chem. C*, 2018, **122**(7), 3809–3817, DOI: 10.1021/acs.jpcc.8b00079.

14 J. Keller, P. Pearson, N. Shariati Nilsson, O. Stolt, L. Stolt and M. Edoff, Performance Limitations of Wide-Gap (Ag,Cu)(In,Ga)Se_2 Thin-Film Solar Cells, *Sol. RRL*, 2021, 2100403, DOI: 10.1002/solr.202100403.

15 R. Gutzler, W. Witte, A. Kanevce, D. Hariskos and S. Paetel, V_{oc}-losses across the band gap: Insights from a high-throughput inline process for CIGS solar cells, *Prog. Photovolt.: Res. Appl.*, 2023, **31**(10), 1023–1031, DOI: 10.1002/pip.3707.

16 F. Larsson, N. S. Nilsson, J. Keller, C. Frisk, V. Kosyak, M. Edoff and T. Törndahl, Record 1.0 V open-circuit voltage in wide band gap chalcopyrite solar cells, *Prog. Photovolt. Res. Appl.*, 2017, **25**(9), 755–763, DOI: 10.1002/pip.2914.

17 R. Gutzler, A. Kanevce, T. Wahl, C. Wessendorf, W. Hempel, E. Ahlswede, D. Hariskos and S. Paetel, Advantage of Zn(O,S) Over CdS Buffer for Low-Gap (Ag,Cu)(In,Ga)Se_2 in Tandem Applications, *ACS Appl. Energy Mater.*, 2024, **7**, 3108, DOI: 10.1021/acsaem.3c03054.

18 D. Regesch, L. Gütay, J. K. Larsen, V. Deprédurand, D. Tanaka, Y. Aida and S. Siebentritt, Degradation and passivation of $CuInSe_2$, *Appl. Phys. Lett.*, 2012, **101**(11), 112108, DOI: 10.1063/1.4752165.

19 F. Babbe, L. Choubrac and S. Siebentritt, Quasi Fermi level splitting of Cu-rich and Cu-poor Cu(In,Ga)Se_2 absorber layers, *Appl. Phys. Lett.*, 2016, **109**(8), 082105, DOI: 10.1063/1.4961530.

20 P. Würfel, The chemical potential of radiation, *J. Phys. C: Solid State Phys.*, 1982, **15**(18), 3967–3985, DOI: 10.1088/0022-3719/15/18/012.

21 S. Siebentritt, U. Rau, S. Gharabeiki, T. P. Weiss, A. Prot, T. Wang, D. Adeleye, M. Drahem and A. Singh, Photoluminescence assessment of materials for solar cell absorbers, *Faraday Discuss.*, 2022, **239**, 112–129, DOI: 10.1039/D2FD00057A.

22 S. Siebentritt, T. P. Weiss, M. Sood, M. H. Wolter, A. Lomuscio and O. Ramirez, How photoluminescence can predict the efficiency of solar cells, *J. Phys. Matter*, 2021, **4**(4), 42010, DOI: 10.1088/2515-7639/ac266e.

23 M. H. Wolter, R. Carron, E. Avancini, B. Bissig, T. P. Weiss, S. Nishiwaki, T. Feurer, S. Buecheler, P. Jackson, W. Witte and S. Siebentritt, How band tail recombination influences the open-circuit voltage of solar cells, *Prog. Photovolt.: Res. Appl.*, 2022, **30**(7), 702–712, DOI: 10.1002/pip.3449.

24 U. Rau and J. H. Werner, Radiative efficiency limits of solar cells with lateral band-gap fluctuations, *Appl. Phys. Lett.*, 2004, **84**(19), 3735–3737, DOI: 10.1063/1.1737071.

25 U. Rau, B. Blank, T. C. M. Müller and T. Kirchartz, Efficiency Potential of Photovoltaic Materials and Devices Unveiled by Detailed-Balance Analysis, *Phys. Rev. Appl.*, 2017, **7**(4), 44016, DOI: 10.1103/PhysRevApplied.7.044016.

26 S. Gharabeiki, F. Lodola, T. Schaaf, T. Wang, M. Melchiorre, N. Valle, J. Niclout, M. Ali, Y. Hu, G. Kusch, R. A. Oliver and S. Siebentritt, The effect of a band gap gradient on the radiative losses in the open circuit voltage of solar cells, *arXiv*, preprint, arXiv:2503.14077, DOI: 10.48550/arXiv.2503.14077.

27 R. Fonoll-Rubio, S. Paetel, E. Grau-Luque, I. Becerril-Romero, R. Mayer, A. Pérez-Rodríguez, M. Guc and V. Izquierdo-Roca, Insights into the Effects of RbF-Post-Deposition Treatments on the Absorber Surface of High Efficiency Cu(In,Ga)Se_2 Solar Cells and Development of Analytical and Machine Learning Process Monitoring Methodologies Based on Combinatorial Analysis, *Adv. Energy Mater.*, 2022, (12), 2103163, DOI: 10.1002/aenm.202103163.

28 C. Spindler, F. Babbe, M. H. Wolter, F. Ehré, K. Santhosh, P. Hilgert, F. Werner and S. Siebentritt, Electronic defects in Cu(In,Ga)Se_2: Towards a comprehensive model, *Phys. Rev. Mater.*, 2019, **3**(9), 90302, DOI: 10.1103/PhysRevMaterials.3.090302.

29 J. Keller, L. Stolt, T. Törndahl and M. Edoff, Silver Alloying in Highly Efficient $CuGaSe_2$ Solar Cells with Different Buffer Layers, *Sol. RRL*, 2023, **7**(12), 2300208, DOI: 10.1002/solr.202300208.

30 J. V. Li, S. Grover, M. A. Contreras, K. Ramanathan, D. Kuciauskas and R. Noufi, A recombination analysis of Cu(In,Ga)Se_2 solar cells with low and high Ga compositions, *Sol. Energy Mater. Sol. Cells*, 2014, **124**, 143–149, DOI: 10.1016/j.solmat.2014.01.047.

31 M. Sood, A. Urbaniak, C. Kameni Boumenou, T. P. Weiss, H. ElAnzeery, F. Babbe, F. Werner, M. Melchiorre and S. Siebentritt, Near surface defects: Cause of deficit between internal and external open-circuit voltage in solar cells, *Prog. Photovoltaics Res. Appl.*, 2022, **30**(3), 263–275, DOI: 10.1002/pip.3483.

32 U. Rau and H. W. Schock, Electronic properties of Cu(In,Ga)Se_2 heterojunction solar cells-recent achievements, current understanding, and future challenges, *Appl. Phys. A*, 1999, **69**(2), 131–147, DOI: 10.1007/s003390050984.

33 S. Siebentritt, E. Avancini, M. Bär, J. Bombsch, E. Bourgeois, S. Buecheler, R. Carron, C. Castro, S. Duguay, R. Félix, E. Handick, D. Hariskos, V. Havu, P. Jackson, H.-P. Komsa, T. Kunze, M. Malitckaya, R. Menozzi, M. Nesladek, N. Nicoara, M. Puska, M. Raghuwanshi, P. Pareige, S. Sadewasser, G. Sozzi, A. N. Tiwari, S. Ueda, A. Vilalta-Clemente, T. P. Weiss, F. Werner, R. G. Wilks, W. Witte and M. H. Wolter, Heavy Alkali Treatment of Cu(In,Ga)Se_2 Solar Cells: Surface versus Bulk Effects, *Adv. Energy Mater.*, 2020, **10**(8), 1903752, DOI: 10.1002/aenm.201903752.

34 O. Ramírez, J. Nishinaga, F. Dingwell, T. Wang, A. Prot, M. H. Wolter, V. Ranjan and S. Siebentritt, On the Origin of Tail States and Open Circuit Voltage Losses in Cu(In,Ga)Se_2, *Sol. RRL*, 2023, **7**(13), 2300054, DOI: 10.1002/solr.202300054.

35 G. D. Cody, T. Tiedje, B. Abeles, B. Brooks and Y. Goldstein, Disorder and the Optical-Absorption Edge of Hydrogenated Amorphous Silicon, *Phys. Rev. Lett.*, 1981, **47**(20), 1480–1483, DOI: 10.1103/PhysRevLett.47.1480.

36 D. Abou-Ras, Microscopic origins of radiative performance losses in thin-film solar cells at the example of

(Ag,Cu)(In,Ga)Se_2 devices, *J. Vac. Sci. Technol., A*, 2024, **42**(2), 022803, DOI: 10.1116/6.0003364.

37 D. Abou-Ras and S. Siebentritt, Erratum: "Microscopic origins of radiative performance losses in thin-film solar cells at the example of (Ag,Cu)(In,Ga)Se_2 devices", *J. Vac. Sci. Technol., A*, 2025, **43**(2), 023403, DOI: 10.1116/6.0004284.

38 S. Gharabeiki, F. Lodola, T. Schaaf, T. Wang, M. Melchiorre, N. Valle, J. Niclout, M. Ali, Y. Hu, G. Kusch, R. A. Oliver and S. Siebentritt, Effect of a Band-Gap Gradient on the Radiative Losses in the Open-Circuit Voltage of Solar Cells, *PRX Energy*, 2025, **4**(3), 33006, DOI: 10.1103/r25l-ftmp.

39 M. Blankenship, D. Hauschild, L. Both, E. Pyatenko, W. Witte, D. Hariskos, S. Paetel, M. Powalla, L. Weinhardt and C. Heske, Conduction Band Cliff at the CdS/$CuIn_{0.1}Ga_{0.9}Se_2$ Thin-Film Solar Cell Interface, *J. Phys. Chem. C*, 2024, **128**(1), 339–345, DOI: 10.1021/acs.jpcc.3c05079.

40 M. Burgelman, P. Nollet and S. Degrave, Modelling polycrystalline semiconductor solar cells, *Thin Solid Films*, 2000, **361–362**, 527–532, DOI: 10.1016/S0040-6090(99)00825-1.

41 T. Kodalle, R. Kormath Madam Raghupathy, T. Bertram, N. Maticiuc, H. A. Yetkin, R. Gunder, R. Schlatmann, T. D. Kühne, C. A. Kaufmann and H. Mirhosseini, Properties of Co-Evaporated $RbInSe_2$ Thin Films, *Phys. Status Solidi RRL*, 2019, (13), 1800564, DOI: 10.1002/pssr.201800564.

42 D. Hauschild, L. Both, M. Blankenship, C. Wansorra, R. Steininger, W. Yang, D. Hariskos, W. Witte, R. Gutzler, M. Powalla, C. Heske and L. Weinhardt, X-Ray and Electron Spectroscopy of the CdS/(Ag,Cu)(In,Ga)Se_2 Interface With RbF Treatment, *Adv. Mater. Interfaces*, 2025, **12**(11), 2401002, DOI: 10.1002/admi.202401002.

43 S. Rühle, Tabulated values of the Shockley–Queisser limit for single junction solar cells, *Sol. Energy*, 2016, **130**, 139–147, DOI: 10.1016/j.solener.2016.02.015.

44 M. A. Contreras, L. M. Mansfield, B. Egaas, J. Li, M. Romero, R. Noufi, E. Rudiger-Voigt and W. Mannstadt, Improved energy conversion efficiency in wide bandgap Cu(In, Ga)Se_2 solar cells, in *37th IEEE Photovoltaic Specialists Conference (PVSC)*, 2011, pp. 26–31, DOI: 10.1109/PVSC.2011.6185837.

45 M. A. Contreras, L. M. Mansfield, B. Egaas, J. Li, M. Romero, R. Noufi, E. Rudiger-Voigt and W. Mannstadt, Wide bandgap Cu(In,Ga)Se_2 solar cells with improved energy conversion efficiency, *Prog. Photovolt.: Res. Appl.*, 2012, **20**(7), 843–850, DOI: 10.1002/pip.2244.

46 G. Hanket, J. H. Boyle and W. N. Shafarman, Characterization and device performance of (AgCu)(InGa)Se_2 absorber layers, in *34th IEEE Photovoltaic Specialists Conference (PVSC)*, Philadelphia, Pennsylvania, USA, 7–12 June 2009; IEEE: Piscataway, NJ, 2009, 2009, pp. 1240–1245, DOI: 10.1109/PVSC.2009.5411241.

47 S. Zahedi-Azad, M. Maiberg and R. Scheer, Effect of Na-PDT and KF-PDT on the photovoltaic performance of wide bandgap Cu (In,Ga)Se_2 solar cells, *Prog. Photovolt.: Res. Appl.*, 2020, **28**(11), 1146–1157, DOI: 10.1002/pip.3317.

48 D. L. Young, J. Keane, A. Duda, J. A. M. AbuShama, C. L. Perkins, M. Romero and R. Noufi, Improved performance in ZnO/CdS/$CuGaSe_2$ thin-film solar cells, *Prog. Photovolt. Res. Appl.*, 2003, **11**(8), 535–541, DOI: 10.1002/pip.516.

49 S. Ishizuka, A. Yamada, P. J. Fons, H. Shibata and S. Niki, Impact of a binary Ga_2Se_3 precursor on ternary $CuGaSe_2$ thin-film and solar cell device properties, *Appl. Phys. Lett.*, 2013, **103**(14), 143903, DOI: 10.1063/1.4823585.

50 J. AbuShama, R. Noufi, S. Johnston, S. Ward and X. Wu, Improved performance in $CuInSe_2$ and surface-modified $CuGaSe_2$ solar cells, in *31st IEEE Photovoltaics Specialists Conference*, 2005, pp. 299–302, DOI: 10.1109/PVSC.2005.1488128.

51 M. Saad, H. Riazi, E. Bucher and M. C. Lux-Steiner, $CuGaSe_2$ solar cells with 9.7% power conversion efficiency, *Appl. Phys. A*, 1996, **62**(2), 181–185, DOI: 10.1007/BF01575717.

52 T. Nakada, K. Yamada, R. Arai, H. Ishizaki and N. Yamada, Novel Wide-Band-Gap $Ag(In_{1-x}Ga_x)Se_2$ Thin Film Solar Cells, *MRS Online Proc. Libr.*, 2004, **865**, 111, DOI: 10.1557/PROC-865-F11.1.

53 K. Kim, S. K. Ahn, J. H. Choi, J. Yoo, Y.-J. Eo, J.-S. Cho, A. Cho, J. Gwak, S. Song, D.-H. Cho, Y.-D. Chung and J. H. Yun, Highly efficient Ag-alloyed Cu(In,Ga)Se_2 solar cells with wide bandgaps and their application to chalcopyrite-based tandem solar cells, *Nano Energy*, 2018, **48**, 345–352, DOI: 10.1016/j.nanoen.2018.03.052.

54 S. Shukla, M. Sood, D. Adeleye, S. Peedle, G. Kusch, D. Dahliah, M. Melchiorre, G.-M. Rignanese, G. Hautier, R. Oliver and S. Siebentritt, Over 15% efficient wide-band-gap Cu(In,Ga)S_2 solar cell: Suppressing bulk and interface recombination through composition engineering, *Joule*, 2021, **5**(7), 1816–1831, DOI: 10.1016/j.joule.2021.05.004.

55 S. Merdes, R. Mainz, J. Klaer, A. Meeder, H. Rodriguez-Alvarez, H. W. Schock, M. Lux-Steiner and R. Klenk, 12.6% efficient CdS/Cu(In,Ga)S_2-based solar cell with an open circuit voltage of 879mV prepared by a rapid thermal process, *Sol. Energy Mater. Sol. Cells*, 2011, **95**(3), 864–869, DOI: 10.1016/j.solmat.2010.11.003.

56 N. Barreau, E. Bertin, A. Crossay, O. Durand, L. Arzel, S. Harel, T. Lepetit, L. Assmann, E. Gautron and D. Lincot, Investigation of co-evaporated polycrystalline Cu(In,Ga)S_2 thin film yielding 16.0% efficiency solar cell, *EPJ Photovoltaics*, 2022, **13**, 17, DOI: 10.1051/epjpv/2022014.

57 H. Hiroi, Y. Iwata, S. Adachi, H. Sugimoto and A. Yamada, New World-Record Efficiency for Pure-Sulfide Cu(In,Ga)S_2 Thin-Film Solar Cell With Cd-Free Buffer Layer via KCN-Free Process, *IEEE J. Photovoltaics*, 2016, **6**(3), 760–763, DOI: 10.1109/JPHOTOV.2016.2537540.

58 N. Barreau, A. Thomere, D. Cammilleri, A. Crossay, C. Guillot-Deudon, A. Lafond, N. Stephant, D. Lincot, M. T. Caldes, R. Bodeux and B. Berenguier, High efficiency solar cell based on Cu(In,Ga)S_2 thin film grown by 3-stage process, in *47th IEEE Photovoltaic Specialists Conference*, 2020, pp. 1715–1718, DOI: 10.1109/PVSC45281.2020.9300598.

59 L. Choubrac, E. Bertin, F. Pineau, L. Arzel, T. Lepetit, L. Assmann, T. Aloui, S. Harel and N. Barreau, On the role of sodium and copper off-stoichiometry in Cu(In,Ga)S_2 for photovoltaic applications: Insights from the investigation of more than 500 samples, *Prog. Photovolt.: Res. Appl.*, 2023, **31**(10), 971–980, DOI: 10.1002/pip.3701.

60 M. Sood, P. Gnanasambandan, D. Adeleye, S. Shukla, N. Adjeroud, R. Leturcq and S. Siebentritt, Electrical barriers and their elimination by tuning (Zn,Mg)O buffer composition in Cu(In,Ga)S_2 solar cells: systematic approach to achieve over 14% power conversion efficiency, *J. Phys.: Energy*, 2022, **4**(4), 45005, DOI: 10.1088/2515-7655/ac8838.